Engineering Structures 196 (2019) 109357

Contents lists available at ScienceDirect

Engineering Structures

journal homepage: www.elsevier.com/locate/engstruct

Quantification of traffic and temperature effects on the fatigue safety of a reinforced-concrete bridge deck based on monitoring data

Imane Bayane[a,*], Amol Mankar[b], Eugen Brühwiler[a], John Dalsgaard Sørensen[b]

[a] EPFL ENAC IIC MCS, Ecole Polytechnique Fédérale de Lausanne, Switzerland
[b] Aalborg University, Thomas Manns Vej, 23, 9220 Aalborg, Denmark

ARTICLE INFO

Keywords:
Fatigue
Reinforced Concrete (RC)
Existing road bridge
Traffic
Temperature
Inverse method
Monitoring

ABSTRACT

For assessment of existing reinforced-concrete bridges, only few rules and recommendations are available, and engineers meanwhile apply design codes for new bridges to evaluate the fatigue safety of existing bridges leading to non-realistic approaches and conclusions. Design codes for new structures are often based on the worst scenarios, and they are not made to assess existing structures with specific loadings and material properties. Direct monitoring provides an important source of information about the actual structural loading and response. This article presents an integral approach to identify fatigue damage of a reinforced-concrete deck as a function of the relevant actions for fatigue using monitoring data. This includes a long-term monitoring system to measure strain and temperature in the most loaded parts, an inverse method using monitoring data to reconstruct traffic actions from the structural response, and a simulation of traffic loading and its effects using a compiler and a finite element model to estimate fatigue damage. The presented approach can be used as a base on how to monitor and analyze recorded data to evaluate the fatigue safety of existing reinforced-concrete slabs in road bridges.

1. Introduction

Reinforced Concrete (RC) is a composite material in which concrete is designed to resist compression stresses and steel reinforcement is designed mainly to resist tensile stresses. Fatigue verification of reinforced-concrete elements requires the examination of both materials, concrete, and steel.

For steel, the fatigue phenomenon has been known as a possible failure cause since the 19th century. Fatigue design rules were introduced particularly with the findings of Wöhler (1867) [1], who recognized that repeated loading far below the ultimate static resistance of a structural element could induce failure [2]. Knowledge about fatigue in metals and other materials has evolved since then.

A century later, fatigue design rules for concrete and reinforced-concrete were introduced in Concrete VB (1974), FIP (1975), TNO-IBBC procedures (1974), DNV rules (1977), NPD regulations (1985), the draft Rules of Concrete Bridges (1988) [3], and SIA (1989) [4].

Most of today's RC bridges were constructed before introducing these rules, and fatigue was not considered during design as a possible failure cause. In Europe, around 75% of RC bridges were constructed before 1988 and in Switzerland, most of them before 1976 [5]. Therefore, there is a need to develop methodologies and approaches to verify the fatigue safety of existing RC bridges.

In the findings of State of the Art Report 188 [6], 17 cases of RC structural elements mainly bridge decks from all around the world (Japan, Sweden, Holland, Germany, United Kingdom, and the United States), were reported where fatigue was the main factor contributing to the deterioration of the structural elements.

For road bridges, RC decks are the most fatigue vulnerable part due to the pronounced effect of axle loads [7–11]. Different experiments and simulations were conducted on reinforced-concrete slabs under moving loads to investigate the fatigue failure mode [12–17]. Fatigue life prediction of RC decks was found to be a challenging task because it is affected by various sources of uncertainties, including material properties, vehicle loads, structural responses and environmental conditions. Therefore, one effective way to cover all these uncertainties comprises the direct monitoring on structures. Structural analysis implementing load-models from standards is not a reliable approach to examine existing RC decks. The load models of the standards are conservative since they do not rely on actual loading and actual structural conditions. In contrast, monitoring provides explicit information about the structural response and thus reduces most uncertainties of parameters related to fatigue safety investigation.

This paper presents a probabilistic methodology to verify the fatigue

* Corresponding author. Tel.: +41 021 693 32 93.
E-mail address: imane.bayane@epfl.ch (I. Bayane).

https://doi.org/10.1016/j.engstruct.2019.109357
Received 21 December 2018; Received in revised form 27 June 2019; Accepted 28 June 2019
Available online 04 July 2019

safety of existing RC slabs, based on data obtained from monitoring. The originality of this work includes:

- The development of an inverse method to identify the position and load of traffic from long-term monitoring data.
- The quantification of the effect of vehicle position and load, as well as temperature variations on the fatigue damage of a RC bridge-deck slab.
- The combination of monitoring data, numerical simulations, and probabilistic assessments to define a procedure for fatigue safety verification.

The methodology can be used as a base on how to monitor existing reinforced-concrete decks and how to process data to evaluate their fatigue safety. It will be illustrated by considering an existing bridge, the Crêt de l'Anneau viaduct, in Switzerland.

2. Monitoring

2.1. Description of the monitored structure

Crêt de l'Anneau viaduct built in 1959 is located in Switzerland on the cantonal road 10, 20 km away from the French border (Fig. 1). It is a composite steel-concrete structure with seven typical spans of 25.6 m and one 15.8 m approach span, for a total length of 195 m. The viaduct is composed of a reinforced-concrete slab fixed on two steel-box-girder beams of 1.3 m height and of variable thickness ranging in the transverse direction from 24 cm near the supports to 17 cm at mid-span. The spans linked to each other by hinges and supported by the piers located 5 m away from each hinge (Fig. 2).

The RC slab was cast with concrete containing 350 kg of cement per m^3; its cube strength was equal to 45 N/mm^2 at 28 days. The deck slab has orthogonal grid reinforcements in both tensile and compression zones with diameters of 10 mm, 14 mm, and 18 mm. A single layer of reinforcement consisting of 25 ϕ10 @200 was provided in the longitudinal direction and 5 ϕ10 @240 in the transverse direction on the compression side. On tensile side, a single layer of reinforcement consisting of 5 ϕ14 @l/3 and 20 ϕ14 @6/m was provided in the longitudinal direction, 10 ϕ14 @106.66 and 2 ϕ18 @l/3 in the transverse direction. A compression-tensile strength of 300 N/mm^2 is assumed for rebars and 235 N/mm^2 for the steel girder.

2.2. Description of the monitoring system

The monitoring system used to investigate the fatigue safety of the RC slab is a system of non-destructive measurements, composed of strain gauges and thermocouples. It is cost-effective, easy to install, use and maintain. It is accessible to any engineering company.

The monitoring system implements recent technologies in data storage and high-frequency acquisition to perform continuous real-time monitoring of the structural response due to action effects mainly traffic loading and temperature. It is implemented for occasional inspections as well as for long-term monitoring. The bridge structure was instrumented in June 2016 with the monitoring system to measure strain and temperature histories at two main spans 2 and 4 (Fig. 2).

Transverse strains were measured by means of two strain gauges installed in the transverse rebars at the mid-span of Slabs 2 and 4 (Fig. 2). Longitudinal strains were measured by two strain gauges installed in the longitudinal rebars at mid-span of the same Slabs 2 and 4 and via one strain gauge installed in the steel girder beam at the mid-span of Slab 4. To monitor the variation of temperature, three thermocouples were installed, namely in the concrete of the slab, on the steel girder and in the air (Fig. 3).

The monitoring system has been operating since June 2016. 44 GB of data were collected and analyzed during the first year of monitoring. The data were recorded continuously with a sampling frequency of 50 and 100 Hz for strain and 2 and 1 Hz for temperature. Every 24 h a binary file was created and stored in the server. It was converted afterward to a Matlab file to process the data.

2.3. Description of the load test

A load test was carried out after the instrumentation of the structure using a five-axle truck with the maximum legal load of 400 kN. LVDT (Linear Variable Differential Transformer) sensors were installed in the instrumented slabs to evaluate the deflection of the cross-section. Four truck passages per direction were performed. The truck speed was varying from 80, 40, 35 to 10 km/h. The five axles of the truck were separately weighted and their actions on the viaduct identified.

Transverse rebars were under tensile stresses during the passage of the truck. In the longitudinal direction, the girder and the longitudinal rebars showed the expected stress reversal, i.e., both tensile and compressive stresses due to vehicle passage (Fig. 4). The five peaks in the longitudinal response represent the passage of the five axles of the truck. The measured strains were mainly influenced by the truck position and by the slab slenderness that accentuates local strains under the wheels.

Identical structural responses were obtained from passages that follow the same trajectory.

The axle configuration of the load-test truck does not have any

Fig. 1. View of the investigated steel-concrete composite viaduct.

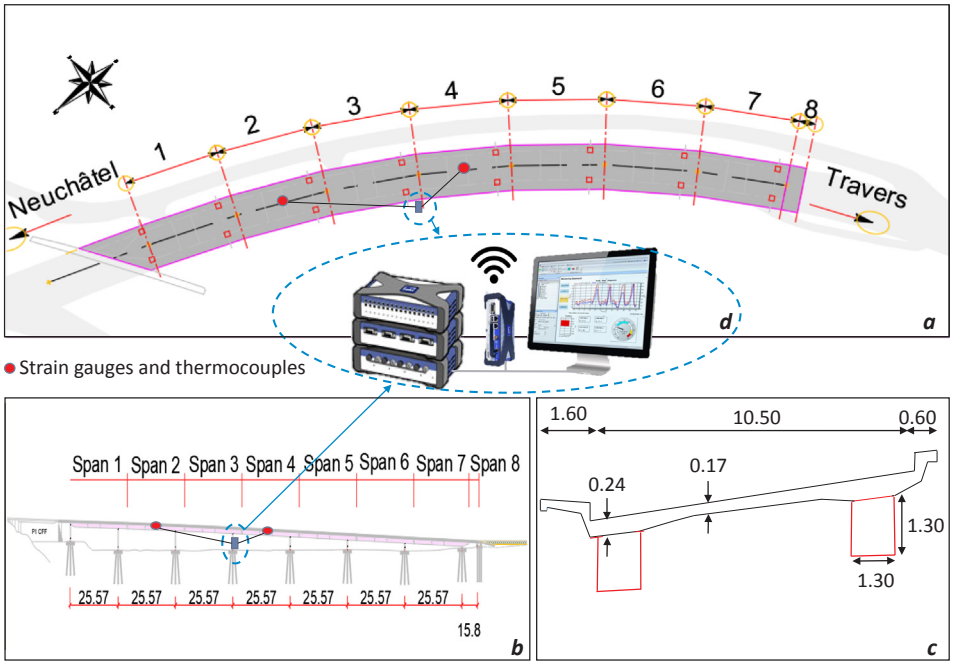

Fig. 2. Drawing of the viaduct (a) plan view; (b) elevation side; (c) typical cross-section; (d) data acquisition and storage unit; dimensions in [m].

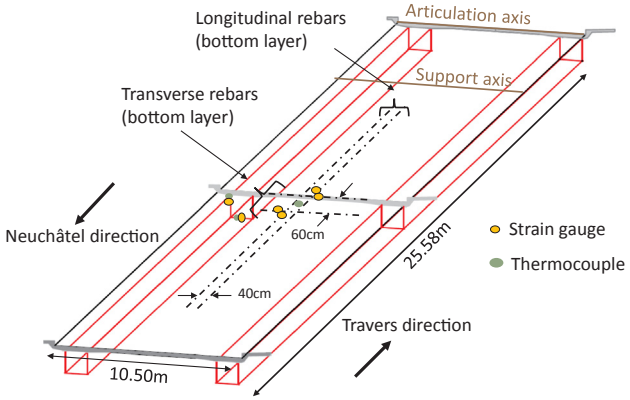

Fig. 3. Location of the sensors in span 4.

influence on the response of the transverse reinforcement and the steel girder, which means that the effect of vehicles can be directly related to their total load when analyzing the structural response of the cross-section.

The results of the load test serve as a base for performing an inverse method to identify traffic features from the recorded strain.

3. Relevant fatigue actions

3.1. Traffic

3.1.1. Approach

An inverse method was developed to identify traffic features from the recorded strain. The results of the load test were used to correlate the strain with the position and the load of the vehicles. Weight In Motion (WIM) data, collected from the same road about 1 km away from the viaduct was used to confirm the results of the inverse method and to evaluate traffic loads in the past and future [18,19]. The long-term statistical distributions of the load and position of all the vehicles crossing the bridge-structure were then established for an assumed 120 years of service duration.

3.1.2. Identification of vehicles

A Peak Over Threshold (POT) approach was applied to the recorded strain to identify all light vehicles and heavy trucks crossing the bridge. Minimum peaks to be included in the dataset were chosen to be above the measurement error, which is 1 μm/m, and the minimum time between each peak was set to 3 s such that, only one peak is identified per vehicle (Fig. 5). The threshold of 1 μm/m eliminates motorbikes and very light cars that are not relevant for structural safety.

This method was applied to strain measurements of the

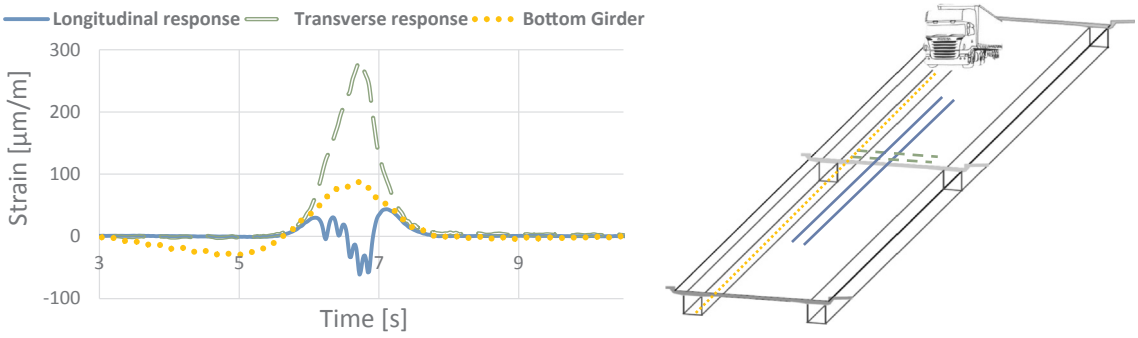

Fig. 4. Strain variations due to a moving load (35 km/h).

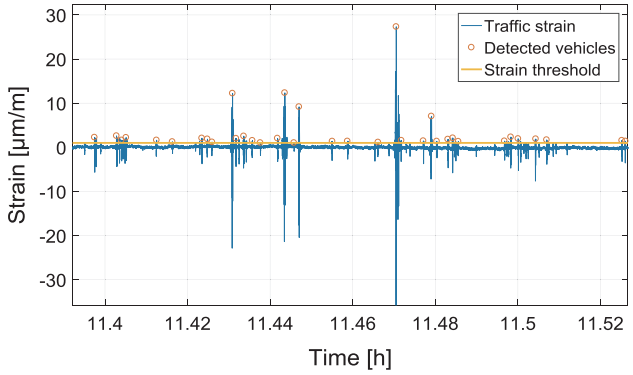

Fig. 5. POT for vehicle identification.

instrumented longitudinal and transverse rebars. A comparison between the identified peaks in each case showed that the longitudinal response has a better representation of the vehicles when comparing with WIM data. The identification of the vehicles was thus performed based on the longitudinal response.

3.1.3. Identification of vehicle position

The roadway width of the viaduct has two lanes, one for respectively the Neuchâtel and Travers directions. To quantify the position of the vehicles, the coordinates of their gravity centre over the width of the roadway are defined as being 0 m for the end of the lane in the Neuchâtel direction, 5.25 m in the centre of the road and 10.5 m for the end of the lane in the Travers direction, as shown in Fig. 6.

During the load test, the truck passed over the viaduct at five positions with respect to the roadway width. Strains in the rebars (transverse and longitudinal) and the girder versus the five positions of the truck are analyzed to determine an explicit correlation between recorded strains and vehicle positions.

It was found that the strain in the transverse rebars was the most sensitive to the position of the vehicles. To quantify this sensitivity, different combinations between transverse strains versus the positions of the test-truck were analyzed and compared to the measured data. The ratio r of strains $\varepsilon_{transverserebar1}$ and $\varepsilon_{transverserebar2}$ in the two instrumented transverse rebars was the parameter directly related to the position, giving similar values for passages with the same position (Eq. (1)). This ratio is approximately unity when the vehicle is located at the centre of the roadway.

$$r = \frac{\varepsilon_{transverserebar1}}{\varepsilon_{transverserebar2}} \tag{1}$$

The ratio r as a function of the vehicle position was fitted with a

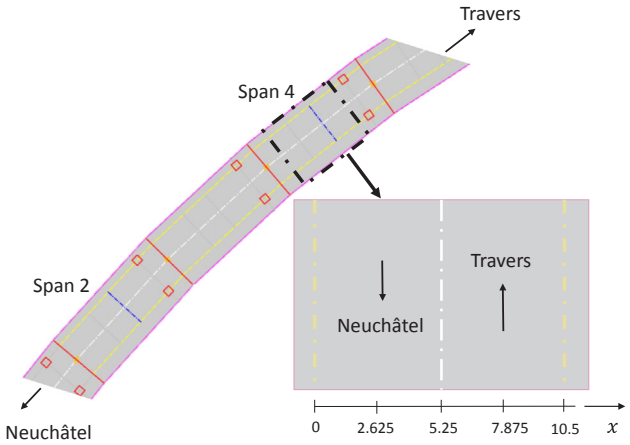

Fig. 6. Vehicle positions in [m] over the roadway width.

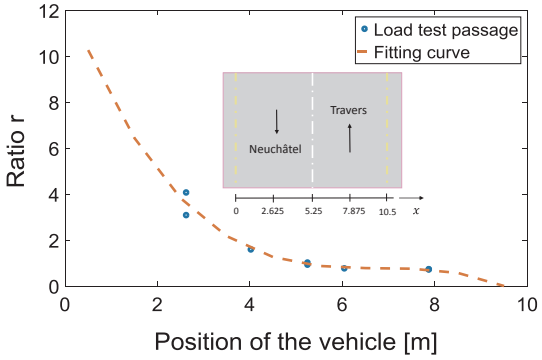

Fig. 7. Fitting curve to calculate the position of the vehicles across the roadway width.

third degree polynomial equation:

$$r = ax^3 + bx^2 + cx + d \tag{2}$$

where x is the position of the vehicle, and a, b, c and, d are the polynomial coefficients, defined from the load-test data. Fig. 7 illustrates the fit of this ratio versus the position of the 400 kN test-truck used to calculate the positions of the detected vehicles.

To obtain the long-term statistical distribution of truck positions, the vehicles were first identified using the peak over threshold approach applied to the longitudinal recorded strains. The corresponding peaks of strains in the two-instrumented transverse rebars were identified, and the ratio r between the peaks was calculated. The real solution of the polynomial $ax^3 + bx^2 + cx + d - r = 0$ corresponds to the position.

The roadway width of the viaduct is 10.5 m, and the wheels of the vehicles can have extreme positions such as 0 m and 10.5 m. The maximum width of the vehicles was assumed as 2 m (Section 3.1.6) and then, in this case, the centre of gravity of the vehicles cannot be less than 1.2 m and cannot be more than 9.3 m. When the calculated position was not in the defined interval, the centre of gravity was directly set at 1.2 m and 9.3 m for the vehicles in the Neuchâtel and Travers directions respectively. The possible positions were then defined in the interval [1.2 m, 9.3 m].

Fig. 8 presents the normalized long-term distribution of vehicle positions over the roadway width.

An increment of 0.1 m was used to define this discrete distribution for the possible positions in the interval [1.2 m, 9.3 m]; as such, 82 positions were defined with their normalized probability of occurrence.

There are three clear peaks for vehicle positions. The peak in the middle represents the vehicles crossing the road from the centre, which can be due to the important slab-slope of 7% and the bend in the road creating a centrifugal force toward the centre for the light vehicles in the Travers direction. Moreover, the vehicles crossing simultaneously the instrumented slab from different directions can create a ratio r near to unity; accordingly, they are also counted in the middle peak.

The two other peaks represent the vehicles crossing the viaduct from the middle of the lane respectively in the Neuchâtel and Travers directions.

The algorithm is well predicting the position of the vehicles since their number in each direction corresponds to the number of vehicles provided by the WIM data (Section 3.1.5). The vehicles that are not included in the interval [1.2 m, 9.3 m], are not frequent.

3.1.4. Identification of vehicle load

The loads are calculated after the identification of the vehicles and their positions. It is assumed that the load and the corresponding strain follow a linear relationship for a specific position.

This assumption of linearity is supported by the results of the load test, where the deflection and the strain values under the 400 kN test-

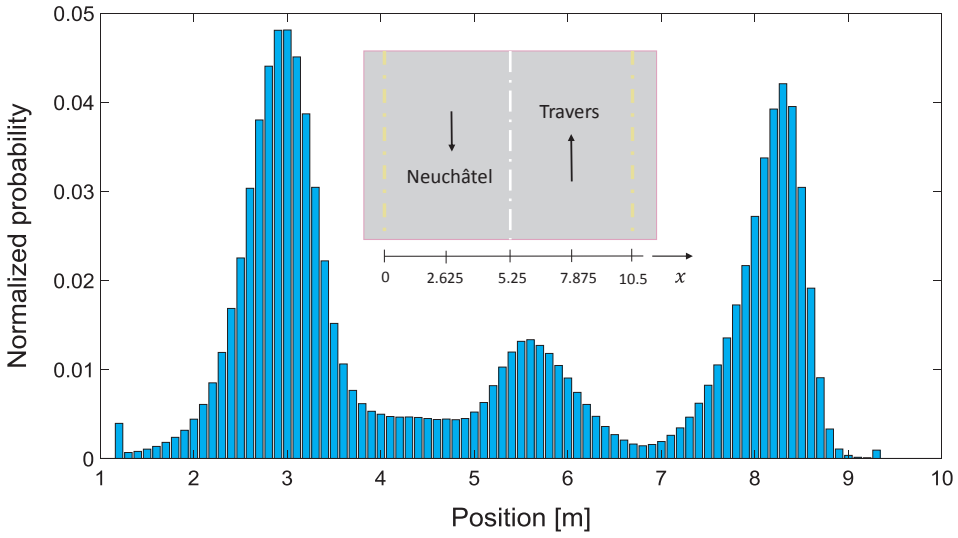

Fig. 8. Normalized annual distribution of vehicle positions.

truck (load limit) regained their initial values after each passage. Moreover, identical structural responses were obtained from passages that follow the same trajectory. The data of the load test contain one set of positions for the same load (400 kN), and they are used to estimate vehicle loads knowing their positions.

The distribution of strain over the roadway width was modeled by a third polynomial fitting of load-test results:

$$\varepsilon(L = 400 \text{ kN} \quad and \quad x = i) = ai^3 + bi^2 + ci + d \tag{3}$$

where ε is the strain due to the passage of vehicle with the load $L = 400$ kN and the position $x = i$, $i \in [1.2m, 9.3m]$.

The response of the girder and the transverse rebars was found to be the most sensitive to truck positions. Therefore, they were used to calculate the load distribution for the 400 kN truck and the identified vehicles according to equation (4).

$$L(x = i) = 400 \text{ kN} \frac{\varepsilon(x = i)}{\varepsilon(L = 400 \text{ kN} \ and \ x = i)} \tag{4}$$

where $\varepsilon(x = i)$ is the recorded strain at the position $x = i$.

Eq. (4) was applied to the recorded strain in the transverse rebars and the girder, and for each vehicle, three loads L were calculated to find the best estimate. Different combinations of the calculated loads were then compared to the WIM data to identify the actual load. Subsequently, the load of the vehicles in the Neuchâtel direction was set equal to the mean of the calculated loads using the strain measured in the girder and the transverse rebar at the mid-span (Eq. (5)). For the Travers direction, the load was directly calculated from the strain measured in the transverse rebar at the mid-span (Eq. (6)).

$$\begin{aligned} L(x = i)_{Neuchâtel} &= 400 \text{ kN} \frac{1}{2} \\ &\left(\frac{\varepsilon_{transverserebar}(x = i)}{\varepsilon_{transverserebar}(L = 400 \text{ kN} \ and \ x = i)} \right. \\ &\left. + \frac{\varepsilon_{girder}(x = i)}{\varepsilon_{girder}(L = 400 \text{ kN} \ and \ x = i)} \right) \end{aligned} \tag{5}$$

$$L(x = i)_{Travers} = 400 \text{ kN} \left(\frac{\varepsilon_{transverserebar}(x = i)}{\varepsilon_{transverserebar}(L = 400 \text{ kN} \ and \ x = i)} \right) \tag{6}$$

Eqs. (5) and (6) were applied to analyze one year of measurements and establish the normalized annual distribution of vehicle loads. An increment of 10 kN was used to represent this discrete distribution, and overall 64 load categories were identified with their normalized probability of occurrence, see (Fig. 9).

The developed algorithm is efficient for the identification of the composition of traffic based on the measured structural response. The resulting traffic distribution reveals that more than 96% of all detected vehicles are cars or small trucks, and 4% are heavy trucks (with a load more than 35 kN). Overloaded trucks exceeding the limit of 400 kN are identified with their position, their velocity and the time they crossed the viaduct. One hundred ten trucks did not respect the 400 kN legal limit over the first year of monitoring with the heaviest recorded load of 640 kN. The heavy trucks represent 8.10^{-5} of all detected vehicles and were frequent during October 2016 for the Neuchâtel direction and during June-July 2017 for the Travers direction, and almost absent during December and January. They were crossing the viaduct mostly from the centre of each lane.

The efficiency of the inverse method depends on the location of strain gauges and their number. It is important to design the position of the gauges over the longitudinal and the cross sections and to choose their numbers. The sensors should provide first, the strain in the most loaded parts to verify the structural safety (with respect to fatigue in the mid-span for the present study). Secondly, four aligned and separated strain gauges for the cross-section are necessary to detect the position of the vehicles in each lane, assuming that the road-bridge has two directions. Finally, two separated strain gauges in the longitudinal section are essential to detect the vehicles and calculate their velocity.

3.1.5. Validation and calibration using WIM data

The WIM-data collected from the local territorial development department [19] was used to validate and calibrate the results of the inverse method (Tables 1 and 2).

The WIM system was installed 1 km away from the viaduct, on the last week of September 2017 (from Monday 25 September to Sunday 1 October). It provided one week of continuous measurement of light and heavy traffic, which represents a solid database to verify the results of the inverse method.

The results of the inverse method were calibrated by the introduction of a calibration factor, equal to the ratio of the results of the inverse method and the WIM data. The weekly number of vehicles for each direction was used to calculate this factor, and accordingly, the number of daily vehicles was calibrated (Tables 1 and 2). An error estimate was calculated as the ratio of the difference between WIM data and calibrated results of the inverse method, and the WIM data.

Light vehicles such as cars of less than 35 kN and motorcycles identified by the established algorithm are not matching with WIM data because most of these vehicles have strain peaks in the domain of error of measurements, i.e., 1 μm/m. This number can easily be matched by

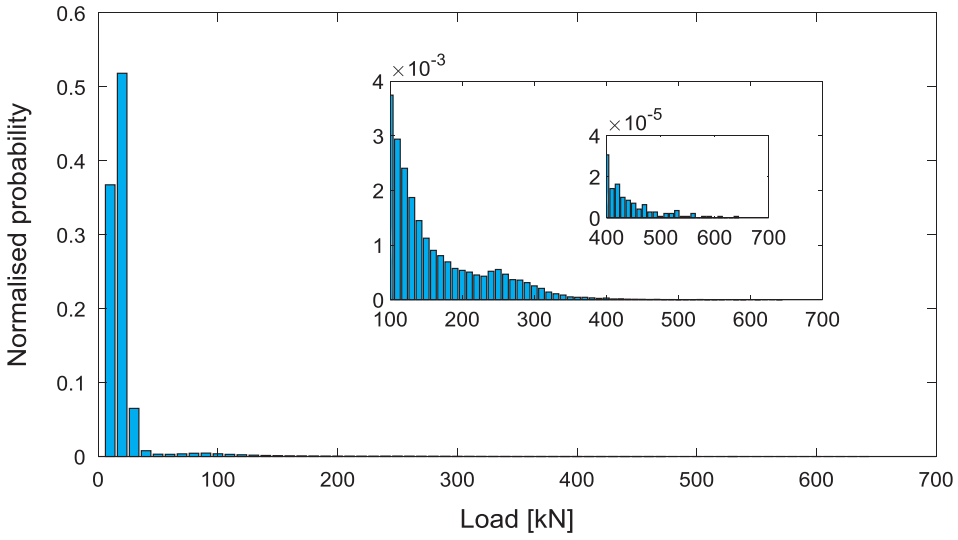

Fig. 9. Normalized annual distribution of vehicle load.

changing the threshold of the POT approach or simply by introducing the missing vehicles. These underestimated vehicles can be neglected compared to other vehicles for the following case study. This assumption is justified in the result section (Section 5).

The error in the estimation of the heavy trucks during the weekend is big. This is due to their small number leading to an increase in the ratio used to calculate the error. In fact, by comparing the detected number of trucks directly, the difference between the WIM data and the inverse method is not important. Moreover, verifying the load of these trucks showed that they are near 35 kN used to separate heavy trucks from light vehicles. Therefore, the error of detection can also be due to the WIM system during the classification.

The load and the position of the vehicles were evaluated by comparing the calculated and the measured numbers of heavy trucks for each direction. It was found that the inverse method provides the correct number of heavy trucks in the Neuchâtel direction, and overestimates the number in the Travers direction. This is mainly due to the use of only one strain gauge response to calculate vehicle loads in the Travers direction. In fact, a more reliable prediction can be achieved in the future by installing a strain gauge in the non-instrumented girder to obtain the transverse response of two aligned strain gauges for each direction. This overestimation was corrected by introducing a factor reducing the difference between the data of the model and the WIM data. The calculated and the measured daily number of heavy trucks in the Travers direction were evaluated, and the daily average of overestimation was identified as 42%. Therefore, the calculated number of heavy trucks ($N°$(heavytraffic))was reduced by introducing a factor of 0.7 (=1/1.42) (Eq. (7)).

$$N°(heavy\ \ traffic)_{corrected} = 0.7N°(heavy\ \ traffic)_{calculated} \quad (7)$$

After the calibration of the results using one week of local continuous WIM data, the robustness of the model was evaluated using continuous monthly WIM data and some daily data recorded during the same period of monitoring (July 2016 to July 2017). The data were collected from the Federal Roads Office FEDRO in Switzerland [18], where the WIM system was installed on the same road, few kilometers far away from the viaduct. To use the provided data, a coefficient of 1.47 was applied to reduce the difference between the FEDRO WIM data and the local WIM corresponding to the traffic crossing the viaduct, according to equation (8).

$$\frac{N°(traffic)_{localWIM}}{N°(traffic)_{FEDRO}} = 1.47 \quad (8)$$

The results of the inverse method were compared with the FEDRO WIM data. The calculated and the measured monthly averages of light vehicles and heavy trucks, and the daily averages of the most loaded days were similar. The calibrated model is efficient for predicting the load and the position of the vehicles.

3.1.6. Traffic growth

Local WIM data [19] and FEDRO data [18] were used to define traffic growth. The data provided the evolution of the annual traffic since 2002 for the same cantonal road X10. Fig. 10 includes the ratio of traffic evolution for the collected data with a linear fitting curve

Table 1
Detected light vehicles according to the WIM data and the inverse method.

Light vehicles								
	WIM data		Inverse method				Error	
			Before calibration		After calibration		After calibration	
Direction	Travers	Neuchâtel	Travers	Neuchâtel	Travers	Neuchâtel	Travers	Neuchâtel
Monday	4124	4217	2418	2439	4256	4293	−3%	−2%
Tuesday	4322	4384	2403	2531	4229	4455	2%	−2%
Wednesday	4408	4436	2508	2546	4414	4481	0%	−1%
Thursday	4544	4644	2538	2591	4467	4560	2%	2%
Friday	4678	4826	2618	2684	4608	4724	1%	2%
Saturday	3363	3477	2113	2250	3233	3443	4%	1%
Sunday	2574	2597	1744	1753	2668	2682	−4%	−3%
Total	28,013	28,581	16,342	16,794	27,875	28,638	0%	0%

Table 2
Detected heavy trucks according to the WIM data and the inverse method.

Heavy trucks								
	WIM data		Inverse method				Error	
			Before calibration		After calibration		After calibration	
Direction	Travers	Neuchâtel	Travers	Neuchâtel	Travers	Neuchâtel	Travers	Neuchâtel
Monday	126	119	122	191	122	125	3%	−5%
Tuesday	128	135	164	191	164	148	−28%	−10%
Wednesday	134	130	143	183	143	134	−7%	−3%
Thursday	138	138	141	185	141	137	−2%	1%
Friday	148	132	156	196	156	127	−5%	4%
Saturday	51	46	44	66	44	36	14%	22%
Sunday	29	26	13	23	13	7	55%	73%
Total	754	726	783	1035	783	714	−4%	2%

defining the annual ratio of traffic growth.

Traffic evolution between 2002 and 2016 was defined according to the ratio of the annual increase in traffic, equal to 1.8%. Since no information was available about the traffic in the past and the evolution of traffic in the future, the ratio 1.8% was used to define four traffic scenarios for 120 years of service, from 1957 to 2077 (Fig. 11).

Scenario 1: constant traffic before 2002 and after 2017 and a linear increase between 2001 and 2017.

Scenario 2: linear increase in traffic before 2017 and constant traffic after 2017.

Scenario 3: constant traffic before 2002 and linear increase in traffic after 2002.

Scenario 4: linear-increasing traffic.

The four scenarios of traffic evolution were used to define the annual statistical distribution of traffic based on the results of the inverse method. The normalized probability of the long-term distribution of vehicle positions and loads was assumed constant while changing the annual number of vehicles according to traffic-growth scenarios.

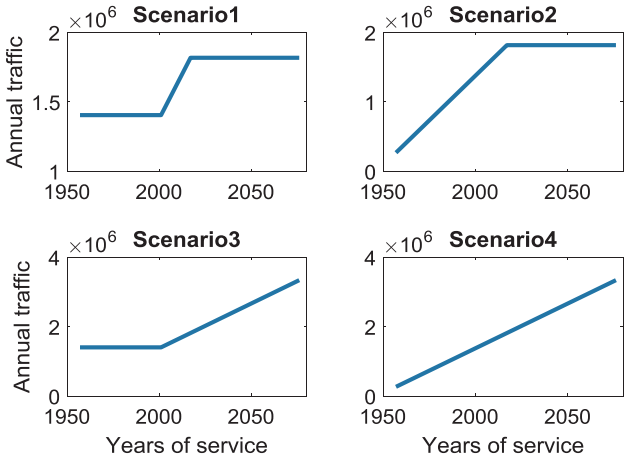

Fig. 11. Scenarios of traffic growth.

3.1.7. The contact surface of vehicles

Axle dimensions and contact surfaces were assumed similar because the local effect of axle dimension was small when simulating the stresses in the finite element model, and the applied loads were correctly diffused in the slab (Section 4). Moreover, the contact surface was modeled only by 2 or 5 axles, since there was not a big difference between the simulated stresses using 2, 3, 4 or 5 axles (Section 4.2).

The vehicles of traffic flow were classified into three categories according to their load to define their surface of contact, used to apply loads in the finite element model.

The first category represents the light vehicles less than 35 kN (cars and small trucks); it was modeled by two axles equally loaded. Heavy trucks more than 35 kN were divided into two categories, two and three. The second category of vehicles with the load range [35, 100 kN] was modeled by two axles loaded differently. The third and last category is for the vehicles heavier than 100 kN, it was modeled by five

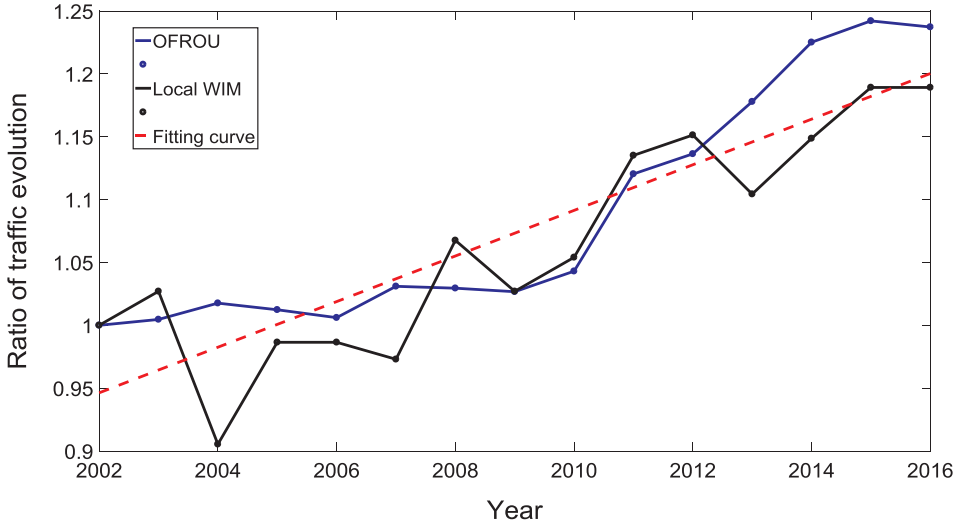

Fig. 10. Ratio of traffic growth from 2002 to 2016.

Table 3
Contact surface of the classified vehicles.

Category		Axles	Contact surface	Axle load distribution	Load category
Light vehicles	1	2	0.4*0.4 m	Equally distributed	[0,35 kN]
Heavy trucks	2	2	0.4*0.4 m	30% and 70%	[35,100 kN]
	3	5	0.4*0.4 m	15%, 15%, 20%, 25% and 25%	[100,700 kN]

axles loaded according to the truck model provided by the Federal Roads Office [20].

The legal limit load of a single axle is 100 kN; therefore, it was defined as the transition from 2 to 5 axles. The details of each category are summarised in Table 3.

The spacing of the axles was also taken from the updated traffic load for concrete deck slabs of existing bridges provided by the federal roads office, as shown in Fig. 12 [20].

The location of the centre of gravity of each category was calculated. This location corresponds to the position provided by the inverse method, used with the defined loads to distribute and load the surfaces of contact for each identified vehicle.

3.2. Temperature

3.2.1. Introduction

The thermal effect on concrete bridges has been widely studied in the literature showing that the contribution of temperature has a significant effect on damage evolution for concrete elements [8,21–24]. Many researches tried to model this effect, particularly [25–27,22]. However, the models were generally subject to many uncertainties, especially when applied to existing bridges, where the state of concrete is not well known. Besides, the thermal gradient is dependent on local conditions. Design codes, for example, present different requirements for each country [24].

Thermal response is, in fact, specific to each bridge and only precise monitoring of temperature and its effect with an explicit analysis of the measured parameters can reduce uncertainties and provide clear information about the structural response due to thermal variations.

For this aim, a detailed study of monitoring data was performed to define the distribution of temperature and thermal strains in the reinforced-concrete slab.

3.2.2. Temperature cycles

Temperature variation is a combination of two cycles, the daily and seasonal cycles. As such, the effect of temperature is a function of two parameters, the period of the day and the period of the year.

To separate these cycles and their effects, a moving average is used in the present case. The daily effect is directly presented with 24 h of measurements for a moving average with a subset of generally 10 min. The seasonal effect is deduced by the moving average with a subset of 30 days.

This processing is outlined in Fig. 13, where the combined, annual and daily cycles of concrete temperature are presented for the Crêt de l'Anneau viaduct.

3.2.3. Temperature effect

Temperature variations can have two direct effects, i.e., thermal diffusivity and thermal expansion.

Thermal diffusivity is the transfer of thermal energy from the warm side to the cold side of the structural element, producing a gradient of temperature that creates a gradient of thermal strain due to thermal expansion. Thermal expansion is presented by the contraction and expansion of materials and is characterized physically by the dilatation coefficient α (Eq. (9)).

$$\varepsilon = \alpha \Delta T \tag{9}$$

where Δε is the thermal strain variation, α the dilatation coefficient [$^{\circ}C^{-1}$], and ΔT the temperature variation [°C].

For concrete and steel, the dilatation coefficient is equal to $10^{-5}\,^{\circ}C^{-1}$.

During monitoring, the configuration of strain gauges is adapted to compensate for the thermal expansion of materials and measure the thermal expansion of structural elements. Stresses due to temperature are in fact, produced when thermal expansion or contraction is restrained in structural elements [26].

This effect is remarkable by its small frequency compared to traffic. Subsequently, the short-term fluctuations due to traffic action effects, and the long-term fluctuations due to temperature effects of time-series data for the recorded strain are separated using a moving average that creates a series of averages for each subset of 10-min. Three signals are resulting as presented in Fig. 14.

Raw data = recorded strain
Thermal strain = moving average of raw data each 10 minutes
Traffic strain = raw data − moving average

The subset of 10 min was chosen by a sensitivity analysis of the structural response. The parameter was modified until obtaining a signal with all the targeted features for traffic strain and thermal strain. Therefore, thermal strains are properly extracted from the recorded data and can be used to evaluate the effect of temperature on fatigue. The probability of occurrence of the recorded temperature and thermal strain within one year of monitoring is normalized, and the annual statistical distributions of temperature and its effect are presented in Fig. 15 for the transverse reinforcement in the mid-span of Slab 4. An increment of 2 μm/m was used to define this discrete distribution for the possible thermal strain of concrete, such that 51 strains were defined with their normalized probability of occurrence. The statistical distribution of temperature and its effect are used to define the mean stress relevant for fatigue reliability investigations for concrete.

4. Numerical simulations

4.1. Finite element model

4.1.1. Approach

A 2-dimensional Finite Element Model (FEM) was developed using the commercial program ANSYS R18.2 for one span of the viaduct, with the purpose of defining the statistical distribution of stresses in the slab

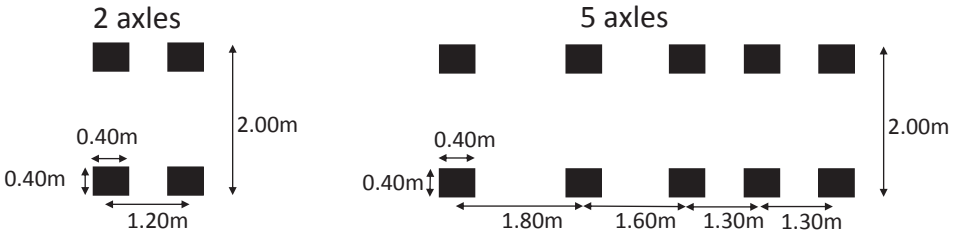

Fig. 12. Spacing of the axles.

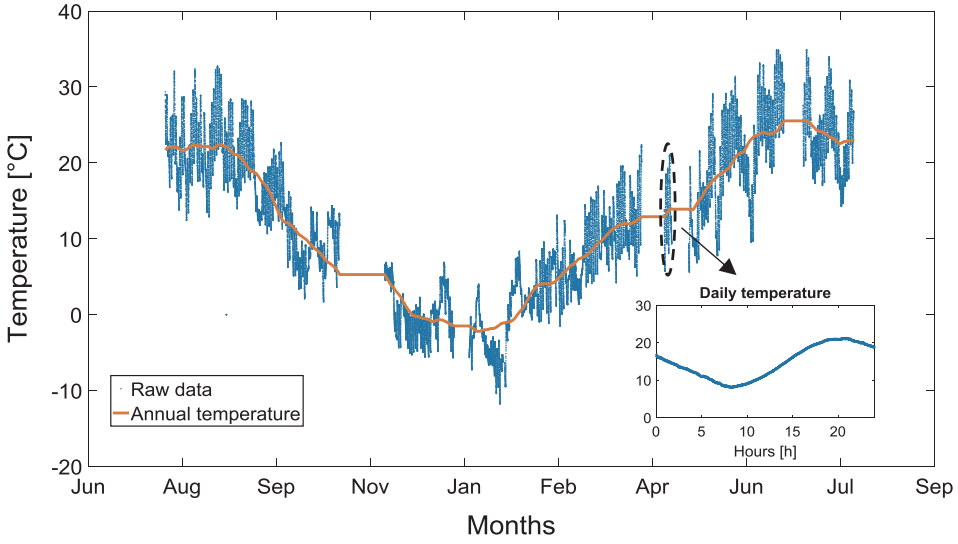

Fig. 13. Annual and daily cycles of concrete temperature.

due to traffic loading.

Numerical models of large civil engineering structures are disposed to uncertain system parameters, which affect the ability of such models to accurately predict the structural response [28]. It is then necessary to develop a detailed finite element model when analyzing the structural response to a specific loading. For this aim, the model was calibrated with monitoring data to reduce the difference between the finite element results and the real-time structural response as obtained by monitoring.

4.1.2. Description of the finite element model

Structural analysis of one span was performed since the seven spans are identical. The concrete and steel were modeled using their initial mechanical properties. To take into account the evolution of material properties during the 60 years of service, the model is calibrated by comparing the simulated strains with the results of the load test. The simulations were performed in the elastic domain.

The element Shell 181 in the ANSYS software was used to model the concrete slab and steel girder. For the slab, an elastic modulus of 35,000 N/mm^2, a Poisson ratio of 0.2, a density of 25 kN/m^3, a compressive strength of 35 N/mm^2 and tensile ultimate strength of 3 N/mm^2 were used.

For the steel girder, an elastic modulus of 210,000 N/mm^2, a Poisson ratio of 0.3 and a compression-tensile ultimate strength of 235 N/mm^2 were used. Material properties are grouped in Table 4.

Mesh density was checked in longitudinal and cross sections by comparing simulated strain for different element sizes. An optimal element size of 100 mm in the longitudinal section and 50 mm in the cross-section were found to give accurate results without time-consuming simulations.

The connection between the reinforced-concrete slab and the girder was assumed a total fixity.

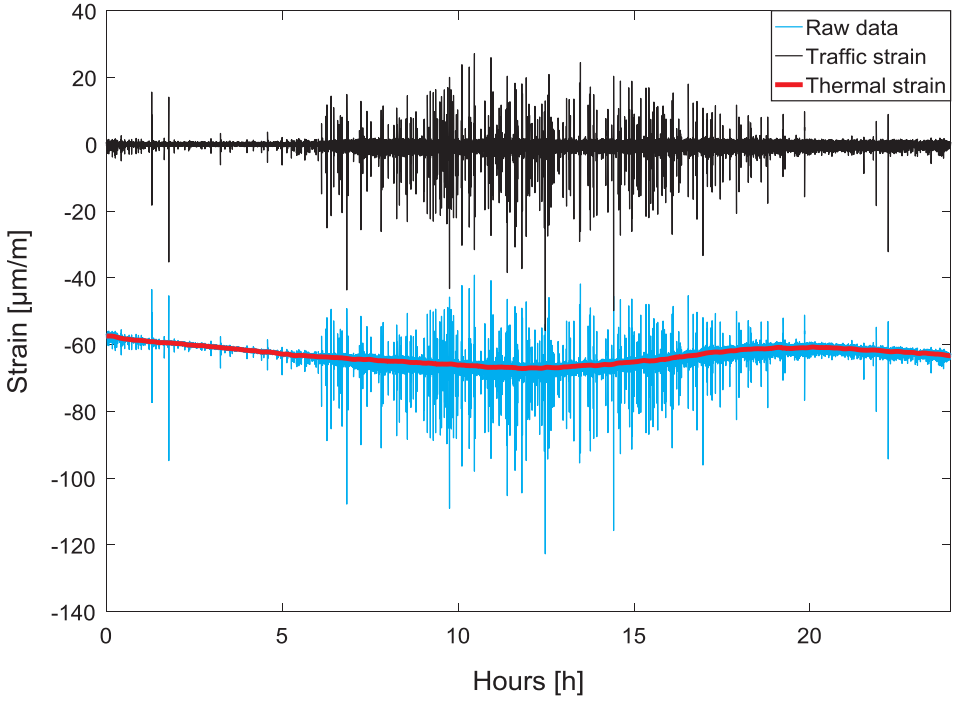

Fig. 14. Daily raw data, thermal strain, and traffic strain.

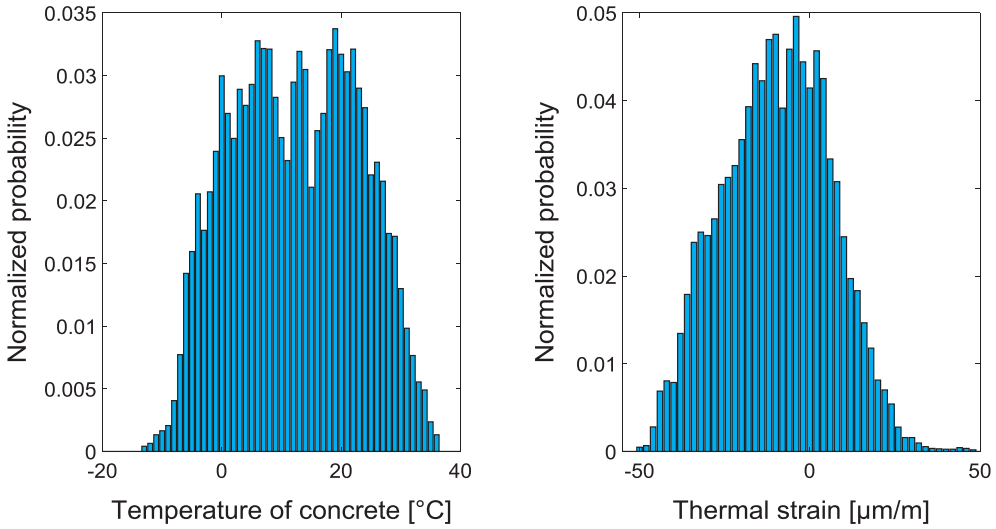

Fig. 15. Normalized annual probability of concrete temperature and thermal strain.

For the boundary conditions, the span was articulated from one side and simply supported as a continuous beam from the other side. The longitudinal displacement and rotations were thus free on one side, and all the displacements and rotations were restricted on the other side.

Fig. 16 includes simulation results for a 5-axle truck with a load of 640 kN on the mid-span.

4.1.3. Calibration of the FE model

The finite element model was calibrated using measured strains and deflections as obtained from the load test. The calibration included changes in material properties, the connections, and the boundary conditions to get the same measured parameters as in the load test [29].

For this case study, the calibration minimizing the difference between monitoring and finite element results was performed in two steps: calibrating strains of the longitudinal section by changing the stiffness, and then calibrating strains and deflection of the transverse section by introducing a calibration factor. Three models are defined: the initial theoretical model, the calibrated model with different stiffness, and the calibrated model with the new stiffness and the calibration factor.

The passages of the 400 kN truck in the centre of the roadway were used for the calibration. The longitudinal response was calibrated by taking the elastic modulus of the concrete as a parameter. It was modified to minimize the difference between the measured and the calculated longitudinal strains.

For the cross-section, a comparison between the results of the non-calibrated finite element model and the load-test model shows that the reinforced-concrete slab is not totally fixed in the steel girder. In fact, the simulated longitudinal strains are identical to monitoring data, but the transverse strains are different. To get closer to real-time measured strains, calibration was proceeded with modeling the elastic flexibility between the girder and the RC slab. This generated some convergence issues due to the use of nonlinear behavior. Therefore, the flexibility between the girder and the slab was introduced by a calibration factor that compensates the difference between the simulated and the measured transverse strain. The calibration factor was found equal to 1.5 to provide the same results as for those obtained by monitoring.

The 2D model was developed to run simulations faster and lighten the calculations while providing the same response of the reinforced-concrete slab as obtained by load test data.

4.2. Simulation and results

Traffic loads are simulated with the toolbox ANSYS_aaS in Matlab providing a direct link between the programs. A Matlab code is developed to run ANSYS commands and save the results for several simulations. Once the deck is modeled, the code generates a new vehicle with a specific load and position, calculates the loads and the positions of the axles, applies the calculated axle loads to the finite element model, runs the model and takes the transverse strain in the mid-span.

The results of the simulation provide the distribution of the strain in the deck for the possible 82 positions and 64 loads.

Fig. 17 includes the distribution of stress ranges in the transverse rebar at the mid-span as a function of vehicle positions and loads. Stress ranges are calculated from the simulated strains using the elastic modulus of steel, 210,000 N/mm^2, and the elastic modulus of concrete, 35,000 N/mm^2.

A small peak can be observed (surrounded by a dashed line), located for stresses under 100kN load, where the passage from two axles to five axles is performed. The peak is present due to the local effect of the applied loads and is more pronounced for two axles. However, this local peak stress is very small and represents less than 1 N/mm^2. As it was highlighted in Section 3.1.7, the number of axles does not induce a significant difference between the simulated stresses. The choice of two axles for loads smaller than 100 kN and five axles for loads higher than 100 kN is thus appropriate.

The simulated and the measured maximum stresses are alike, which proves that the finite element model is well calibrated for the structural response of heavy trucks.

The maximum stresses are due to the heavy trucks located at the mid-span. The trucks create two peaks, 1 m away from the mid-span, which corresponds to the location of the axles.

To define the annual statistical distribution of stresses due to traffic, the position and the load of the vehicles were considered as

Table 4
Material properties.

Material	Density [kN/m^3]	Young's Modulus [N/mm2]	Poisson's Ratio	Element
Reinforced concrete (slab)	25	35,000	0.2	Shell 181
Steel (girder)	78.5	210,000	0.3	Shell 181

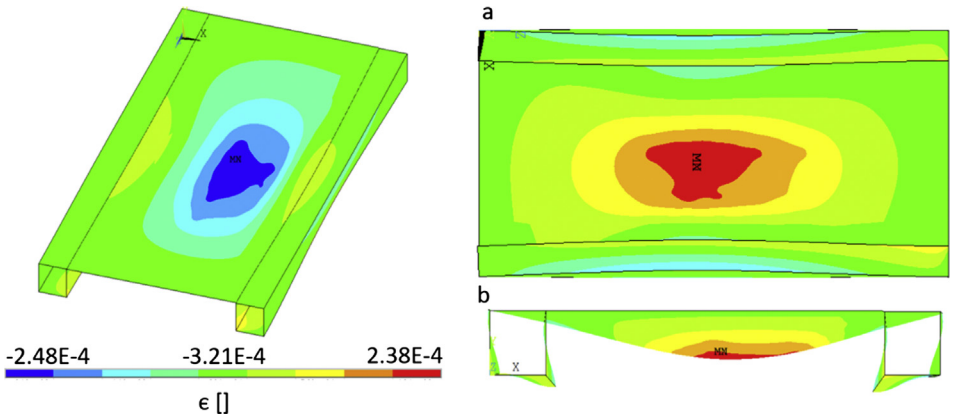

Fig. 16. FEM simulation results of the deck, bottom side (a) and cross-section side (b).

independent stochastic variables. The annual number of cycles with the strain range $\varepsilon_{i,j}$ generated by the vehicle with the position-load $[x_i, L_j]$, is defined from the distributions of the loads and positions (Fig. 8, Fig. 9), according to equation (10).

$$n_{i,j} = P_{x_i} P_{L_j} N \tag{10}$$

where $n_{i,j}$ is the number of vehicles with the position x_i and the load L_j creating the strain range $\varepsilon_{i,j}$

P_{L_j} is the probability that the vehicle has a load L_j

P_{x_i} is the probability that the vehicle is at position x_i

N is the total number of vehicles per year

Fig. 18 provides steps to identify the probabilistic distribution of stresses as a function of the load and the position of the vehicles.

5. Fatigue verification

In this study, the verification of the fatigue safety of the present reinforced concrete slab designed to resist predominantly in the transverse direction is focused on the bending failure mode, which may result either in compression failure of the concrete or tensile failure of the reinforcement.

The recorded strains in the transverse rebars were higher than the strain in the longitudinal rebars, which is mainly due to the distribution of the actual traffic loads on both the RC slab and the steel girder carrying in the longitudinal direction, while in the transverse direction only the 17 cm-thickness RC slab is acting. The mechanism of fatigue failure of reinforced-concrete slabs is complex and depends on many variables (stress ranges, reinforcement ratio, boundary conditions…).

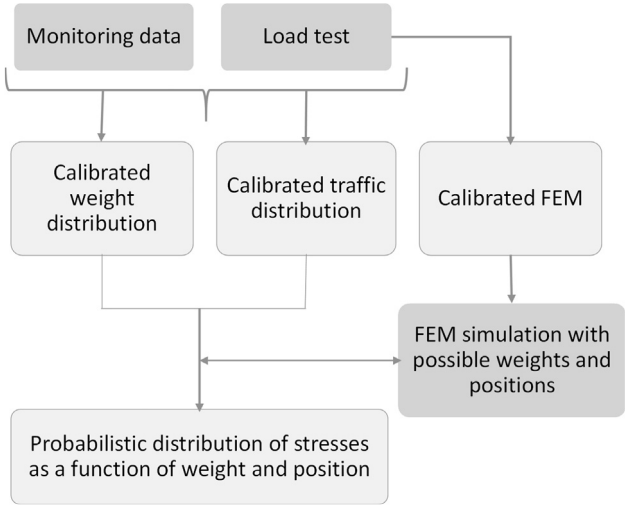

Fig. 18. Steps to define the statistical distribution of traffic stresses.

Previous studies show that the failure can be induced by the interaction of flexural-shear cracks of concrete [12–14] or rebar fracture when there is no longer stress transfer [30,15]. For this study, no concrete cracking was visible in the mid-span of the RC slab, the reversal stresses were present in the longitudinal response as shown in Fig. 4, but were lower than transverse stresses. Even under significant shear fatigue stress, this type of slabs were reported to fail due to fatigue failure of the

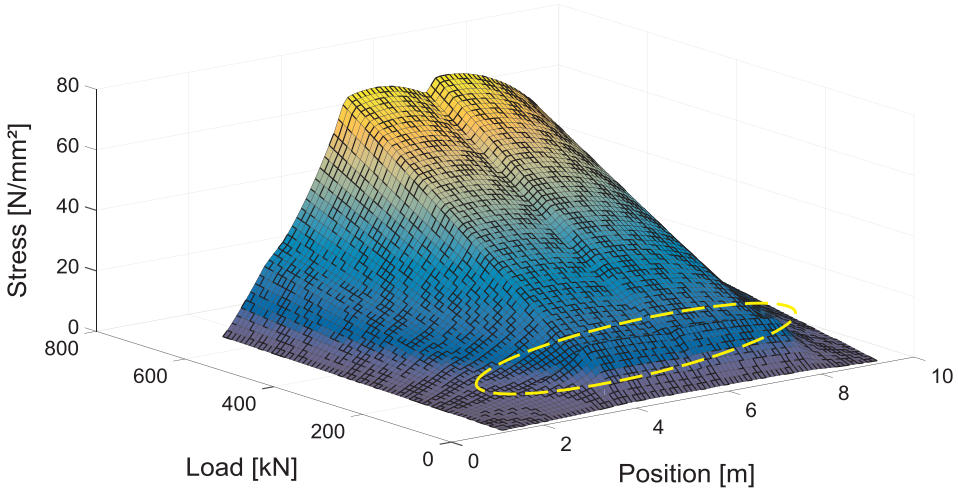

Fig. 17. 3D distribution of the simulated stresses at the mid-span transverse rebar.

rebars [30]. Therefore, the cross-section of the RC slab was defined as the critical section, and the fatigue stress is investigated using the transverse strains. The investigation of the effect of reversal stresses will be presented in future work.

5.1. Fatigue verification of steel reinforcement

Fatigue of steel reinforcement is verified at two levels. The first level requires the verification of the fatigue stresses to be below the endurance limit. Level 2 is performed when Level 1 is not conclusive, and it requires the calculation of the fatigue damage. In the Swiss standard SIA269/2, the fatigue resistance of straight rebars with a diameter less than 30 mm is equal to $\Delta\sigma_{sd,\ fat} = 150\ N/mm^2$ and the endurance limit is equal to 80% of the fatigue limit, i.e., $\Delta\sigma_{sD} = 120\ N/mm^2$, the slope of the S-N curve being equal to m = 4 [31].

The level one is fulfilled for the rebars at the mid-span since all the measured stress ranges are below $120\ N/mm^2$. Therefore, steel reinforcements do not present any fatigue problem based on the one-year monitoring data. The Level 2 of fatigue verification does not need to be performed in this case. However, to illustrate the damage as a function of the actions relevant to fatigue, the recorded stresses are arbitrarily amplified by a factor of 4 to obtain stress values higher than the endurance limit. Subsequently, the Level 2 verification is conducted with fictitious stress values that relate to real loading conditions.

Fatigue damage is quantified in terms of Miner's damage summation to deal with variable amplitude loading in the S-N approach. According to this rule, all stress cycles induce proportional fatigue damage, which is linearly additive. The scatter in the stress history may be neglected and the damage d due to n_i cycles for the stress range $\Delta\sigma_i$ is equal to:

$$d = \sum \frac{n_i}{N_i} \tag{11}$$

where

d	is the cumulative damage
n_i	is the number of cycles for the constant stress$\Delta\sigma_i$
N_i	is the total number of cycles to failure under the constant amplitude stress$\Delta\sigma_i$

The fatigue safety is fulfilled if the accumulated damage is less than 1:

$$d < 1 \tag{12}$$

The damage is calculated according to Eq. (11) using the annual statistical distribution of stresses and stress cycles defined in the previous section. Fig. 19 illustrates the annual distribution of damage for the first year of monitoring as a function of the position and load of vehicles.

The fatigue damage is zero for stresses lower than the endurance limit, which is the case for the vehicles lower than 300 kN, no matter their positions. Only heavy trucks are then relevant for fatigue damage, and the light vehicles can be neglected for the verification of the fatigue safety of steel reinforcement. This justifies the threshold used in the POT approach, discriminating the vehicles that create strain less than 1 μm/m.

Fig. 19 indicates that fatigue damage is more pronounced for the vehicles crossing the roadway from the middle.

The trucks with a load between 350 kN and 400 kN are the most frequent, which is mainly due to the legal load limit for vehicles fixed at 400 kN for this viaduct. The frequency of these trucks creates the highest annual fatigue damage.

The trucks heavier than 400 kN create high fatigue damage. However, they are not frequent, and their annual effect is less pronounced.

To evaluate the accumulated damage during the years of service of the viaduct, and to predict the total damage in the future, the four scenarios of traffic growth introduced in Section 3.1.6 are analyzed. Accordingly, the accumulated damage is calculated for 120 years of service as shown in Table 5.

Even by amplifying the stress ranges arbitrarily with a factor of four, the fatigue damage is small and does not present a significant damage value after 120 years of service, for different scenarios of traffic growth. Consequently, the service duration of the viaduct is very long, with the actual evolution of traffic considering fatigue safety.

The scenarios of traffic growth define the evolution of the accumulated damage. A difference of 40% is present between the non-conservative scenario (2) and the conservative scenario (3). Therefore, the consideration of different scenarios of traffic growth is necessary to quantify the fatigue damage, mainly when no information is available for the past and future traffic.

This inverse method allows evaluating the damage as a function of vehicle position and load. This information may be useful to make decisions about limiting or reducing a particular type of vehicles or imposing certain vehicle positions to restrain fatigue damage. Moreover, this information may also be useful to allow for a controlled increase in the number of vehicles and trucks and the legal vehicle load limit while limiting possible fatigue damage.

5.2. Fatigue verification of concrete

The fatigue of concrete is verified based on the *fib* Model Code [32]. The fatigue requirements under cyclic loading are met if the required lifetime (number of cycles) is lower than or equal to the number of

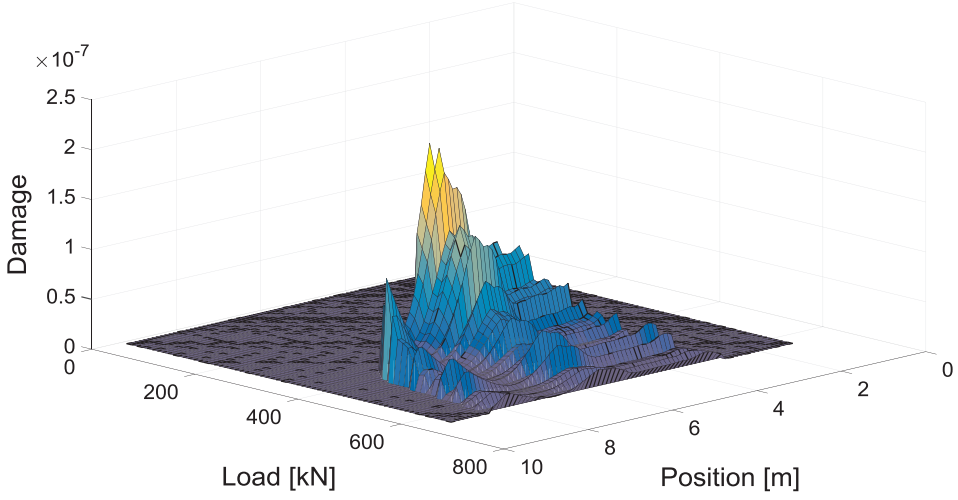

Fig. 19. Annual fatigue damage distribution for the transverse rebar at the mid-span (Monitored stresses are arbitrarily amplified by a factor of four).

Table 5
Accumulated fatigue steel damage for 120 years of service.

Scenario	1	2	3	4
Accumulated damage	$4.80\ 10^{-03}$	$4.20\ 10^{-03}$	$5.90\ 10^{-03}$	$5.30\ 10^{-03}$

cycles to failure.

$$n \leq N \tag{13}$$

n is the foreseen number of cycles during the service duration
N is the number of resisting stress cycles

The recorded strains in the transverse rebars were more than twice the strains of the longitudinal rebars. In fact, in the longitudinal section of the viaduct, the applied traffic loads were distributed across the RC slab and the steel girder, but for the cross-section, axle loads were directly distributed along the 17 cm RC slab. Therefore, the reinforced concrete is verified for the cross-section assuming uniaxial tensile stress in the steel reinforcement rebars, and uniaxial compression stress in the concrete. Assessment of fatigue damage for the concrete under compression is presented in the following.

Fatigue loading of concrete is expressed in [32] by the maximum compressive stress level $S_{c,max}$ and the minimum compressive stress level $S_{c,min}$. Such as, for $S_{c,min} > 0.8$, the S-N relations for $S_{c,min} = 0.8$ are valid, and for $0 < S_{c,min} \leq 0.8$, the following equations apply.

The number of cycles N to failure is obtained from

$$\log N = \log N1 \quad if \quad \log N1 \leq 8 \tag{14}$$

$$\log N = \log N2 \quad if \quad \log N1 > 8 \tag{15}$$

where

$$\log\ N1 = \frac{8}{Y-1}(S_{c,max} - 1) \tag{16}$$

$$\log\ N2 = 8 + \frac{8ln(10)}{Y-1}(Y - S_{c,min})\log\left(\frac{S_{c,max} - S_{c,min}}{Y - S_{c,min}}\right) \tag{17}$$

$$with\ Y = \frac{0.45 + 1.8S_{c,min}}{1 + 1.8S_{c,min} - 0.3S_{c,min}^2} \tag{18}$$

$$S_{c,max} = |\sigma_{c,max}|/f_{ck,fat} \tag{19}$$

$$S_{c,min} = |\sigma_{c,min}|/f_{ck,fat} \tag{20}$$

The fatigue reference compressive strength $f_{ck,fat}$ depends on the age of concrete at the beginning of fatigue loading and it may be estimated from [32]:

$$f_{ck,fat} = \beta_{cc}(t)\beta_{c,sus}(t,\ t_0)f_{ck}(1 - \frac{f_{ck}}{400}) \tag{21}$$

with

N	is the number of cycles to failure
$S_{c,max}$	is the maximum compressive stress level
$S_{c,min}$	is the minimum compressive stress level
$\sigma_{c,max}$	is the maximum acting compressive stress in [MPa]
$\sigma_{c,min}$	is the minimum acting compressive stress in [MPa]
f_{ck}	is the characteristic compressive strength
$f_{ck,fat}$	is the fatigue reference compressive strength
$\beta_{cc}(t)$	Is a coefficient which depends on the age of concrete at the beginning of fatigue loading
$\beta_{c,sus}$	Is a coefficient which takes into account the effect of high mean stresses during loading, for fatigue loading it may be taken as 0.85

β_{cc} represents the 'time-dependant' aspect and it is calculated according to equation (22).

$$\beta_{cc}(t) = \exp[s\left(1 - \sqrt{\frac{28}{t}}\right)] \tag{22}$$

such as s = 0.25, a coefficient which depends on the strength class of cement and t is the concrete age in days.

The RC slab is made with a special concrete CP350, with cube strength equal to 45 N/mm^2 at 28 days. f_{ck} is then equal to 35 N/mm^2 and the elastic modulus is equal to 35 000 N/mm^2 [32].

The maximum compressive stress is equal to the stress due to dead loads, temperature and traffic:

$$\sigma_{c,max} = \sigma_{traffic} + \sigma_{dd} + \sigma_{temperature} \tag{23}$$

The minimum compressive stress is equal to the stress due to dead loads and temperature:

$$\sigma_{c,min} = \sigma_{dd} + \sigma_{temperature} \tag{24}$$

where

$\sigma_{traffic}$	is the stress due to traffic loading
σ_{dd}	is the stress due to dead load
$\sigma_{temperature}$	is the stress due to temperature

Strain values in the concrete are deduced from the calculated strain in the transverse rebar at the mid-span with respect to the neutral axis location of the cross-section. For a non-cracked section, the neutral axis is located at a distance of 87.5 mm from the top. The concrete below the neutral axis is assumed to be cracked [30], and steel reinforcement is taking the tensile stress. Accordingly, the recalculation gives the new location of neutral axis at 45 mm below the top. This neutral axis is subsequently used to calculate concrete stresses due to traffic $\sigma_{traffic}$ as the highest stress at the top of the cross-section using measured strain values.

The stress due to dead loads σ_{dd} is obtained from the finite element model.

The stress due to temperature $\sigma_{temperature}$ is considered as a stochastic independent variable, with a discrete distribution defined from monitoring data (Section 3.2.3, Fig. 15).

Stresses are calculated from strain by multiplying them with the elastic modulus of concrete. To obtain significant fatigue stresses, an arbitrarily chosen multiplication factor of four is again used for the stress values of concrete. Each calculated stress corresponds to the passage of a vehicle with the transverse signature illustrated in Fig. 4, thus, for each calculated stress range corresponds ½ cycle.

The fatigue damage of concrete is calculated as a function of temperature variations and the position and the load of the vehicles.

Fig. 20 illustrates the fatigue damage of concrete as a function of vehicle positions and temperature for a load of$L = 320$ kN, as a function of vehicle load and temperature for the position$x = 2.2$ m, and as a function of the load and the position of the vehicles for the temperature $T = 820$ °C.

Temperature variations influence the fatigue damage of concrete, which takes the same distribution of temperature (Fig. 15) for a fixed load or position. The fatigue damage of concrete increases significantly for loads higher than 400 kN, which means that the heavy trucks create higher fatigue damage even if they are not as frequent as the light vehicles. The damage is higher in the Neuchâtel direction, where the heaviest trucks are more frequent. The accumulated fatigue damage according to the four scenarios of traffic growth is presented in Table 6.

The fatigue damage of concrete due to the past and future traffic is also very small, even after 120 years of service, although the values from monitoring were arbitrarily multiplied by a factor of four. Consequently and despite highly conservative assumptions, the

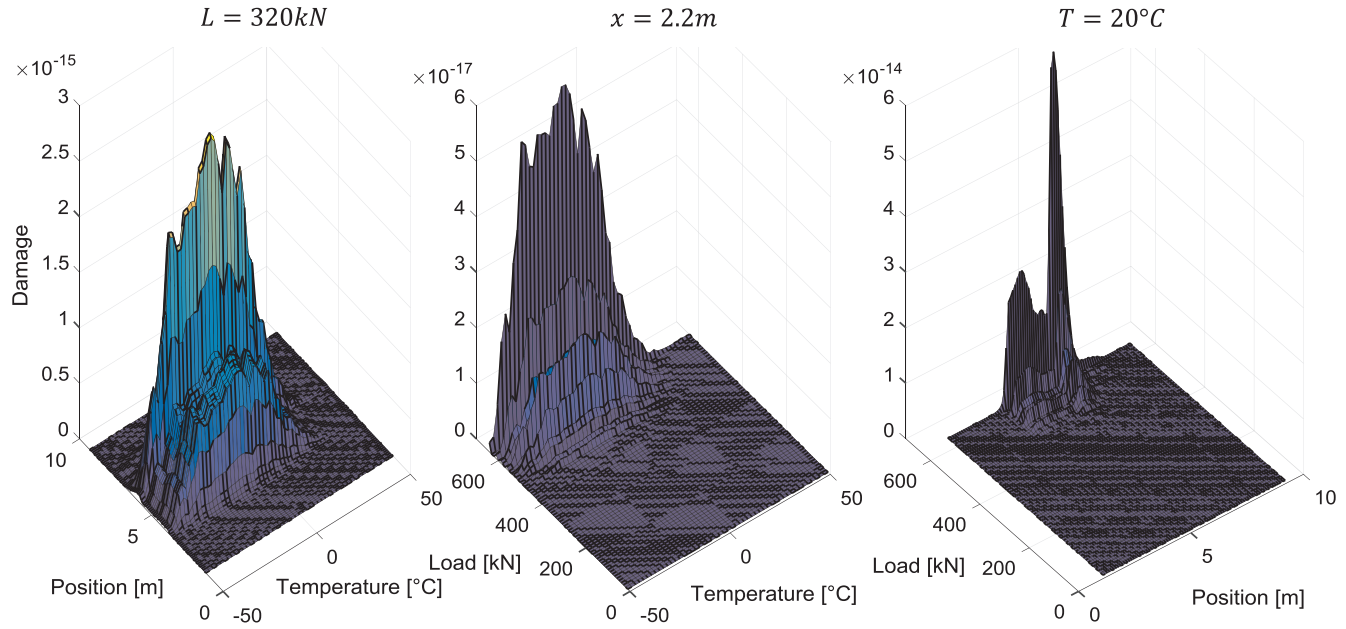

Fig. 20. Long-term fatigue damage distribution of concrete (L = 320 kN, x = 2.2 m, T = 20 °C) (Monitored stresses are arbitrarily amplified by a factor of four).

Table 6
Accumulated fatigue concrete damage for 120 years of service.

Scenario	1	2	3	4
Accumulated damage after 120 years of service	8.90 10^{-04}	7.74 10^{-04}	1.10 10^{-03}	9.81 10^{-04}

concrete of the RC slab does not show any fatigue problem in the present and will not present any notable fatigue issue in the future.

The calculated fatigue damage of concrete is 20% lower than the calculated fatigue damage of steel reinforcement. This means that under pure compression of concrete, the steel reinforcement can be expected to fail first due to tensile cyclic loading. This result coincides with the findings of [10,15,33] where steel rebars failed before concrete under fatigue loading.

5.3. Sensitivity analysis

To understand the interrelation between input parameters and fatigue damage and to identify the parameters that cause significant uncertainties in the calculations, a sensitivity analysis of the fatigue damage of steel and concrete is conducted.

The sensitivity of three main parameters involved in the fatigue damage d calculations is evaluated. The compressive strength of concrete f_{ck}, the stress factor and the annual traffic is varied such that 100% corresponds to their initial values, 35 MPa, 4, and 1 405 502 vehicles/year, respectively (Figs. 21 and 22).

The fatigue damage of steel and concrete presents a linear variation with the annual traffic in terms of vehicle number. In fact, while changing the annual traffic, the position and the load of the vehicles stay constant. The stress ranges are thus the same with different cycles. According to Eq. (11), the fatigue damage is linearly related to the number of stress cycles. Therefore, traffic growth under the same distribution of loads and positions will generate similar growth of fatigue damage.

The fatigue damage of steel is increasing exponentially with the stress factor, while the logarithm of concrete damage and the stress factor are linearly related. The stress factor presents the changes in the stress ranges due to the variation in load and position distributions. Fatigue damage is thus highly sensitive to heavy trucks and the most-loaded positions.

The increase of concrete compression strength creates an exponential decrease in the fatigue damage of concrete. It is then essential to assess the strength of concrete well when evaluating its fatigue safety because it is a critical parameter for fatigue damage.

6. Conclusion

The fatigue safety of the RC slab of a 60-year road viaduct is investigated based on monitoring data, considering the structural response, traffic loads, temperature effect, and their combinations. The main goal of this study is to develop a practical method to evaluate the fatigue safety of RC road bridges. This is particularly significant when using monitoring data that reduces the uncertainties in traffic and environmental load properties and structural response, which is a considerable advantage over design code estimates. For this purpose, the focus was to evaluate the fatigue damage of steel reinforcement and concrete and its evolution in time as a function of temperature variations and the positions and loads of vehicles.

Five main conclusions can be highlighted as follows:

1. The inverse method identifies precisely the loads and positions of all the vehicles that are crossing the RC slab, using data from only four strain gauges and a load test.
2. The combination of FE modeling and probabilistic assessment of monitoring data provides probabilistic distributions of stresses in the RC slab as a function of the load and the position of the vehicles.
3. The comparative verification of both steel reinforcement and concrete identifies the governing material in terms of fatigue safety. Steel reinforcement is governing.
4. Recording ambient temperature and thermal variations of concrete for one year provides reliable data to capture the effect of temperature on concrete fatigue.
5. The sensitivity of fatigue damage to different sources of uncertainties (associated with compressive strength, level of stress and magnitude of annual traffic) is clearly identified.

The results of the inverse method were compared to WIM data and found to be accurate. Hence, the presented methodology can be used to

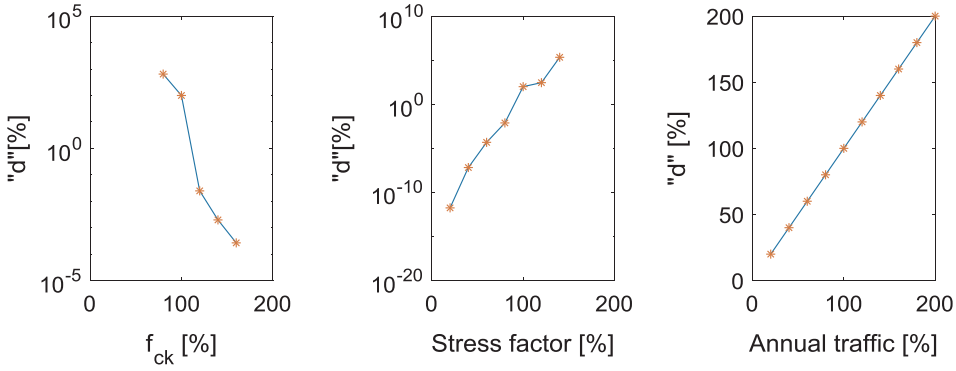

Fig. 21. Sensitivity of the fatigue damage of concrete.

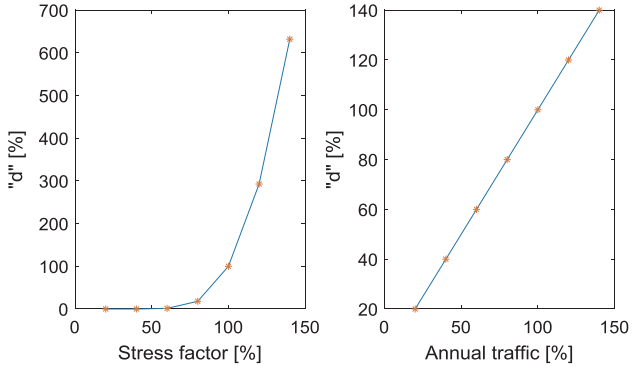

Fig. 22. Sensitivity of the fatigue damage of steel.

verify the RC slabs suspected to have a fatigue problem. The accuracy of the inverse method can be further improved by installing two strain gauges for each lane and direction and performing a load test with different positions, velocities and loads.

The combination of the calibrated finite element model and the probabilistic assessments is demanding. However, it can be updated and used to verify the fatigue safety of the structure for future service duration. Regarding the sensitivity analysis, an extension for the future is to consider it from a reliability point of view, accounting for the uncertainty of the fatigue load and fatigue strength and the influence of the reliability.

Acknowledgments

Current work is carried out under project INFRASTAR (Innovation and Networking for Fatigue and Reliability Analysis of Structures - Training for Assessment of Risk). The project INFRASTAR (infrastar.eu) has received funding from the European Union's Horizon 2020 research and innovation programme under the Marie Skłodowska-Curie grant agreement No 676139.

References

[1] Wöhler A. Wöhler's experiments on the strength of metals. In: Engineering, vol. 4, Lond.; 1867. p. 497–8.
[2] Schijve J. Fatigue of structures and materials. 2nd ed. Netherlands: Springer; 2009.
[3] Siemes AJM, TNO Institue for building materials and structures. Fatigue evaluation of concrete structures preliminary studies, procedure and examples. HERON 1988;33(3):75.
[4] S.I.A. SIA, Ermüdung von Betonbauten. SIA Dokumentation, no. D 0133; 1997.
[5] Fehlmann P. Zur Ermüdung von Stahlbetonbrücken. ETH Zurich; 2012.
[6] CEB, Comité Euro-International du Béton, Fatigue of concrete structures, state of the art, no. 188; 1988.
[7] Spathelf CA. Fatigue performance of orthogonally reinforced concrete slabs. Report: ETH Zurich; 2018.
[8] Treacy MA, Brühwiler E. Action effects in post-tensioned concrete box-girder bridges obtained from high-frequency monitoring. J. Civ. Struct. Health Monit. 2015;5(1):11–28.
[9] Fehlmann P, Vogel T. Experimental investigations on the fatigue behavior of concrete bridges. Sustainable infrastructure : IABSE Symposium, Bangkok 2009. 2009.
[10] Herwig A. Reinforced Concrete Bridges under increased Railway Traffic Loads - Fatigue Behaviour and Safety Measures, PhD Thesis Éc. Polytech. Fédérale Lausanne, no. 4010; 2008.
[11] Schläfli M, Brühwiler E. Fatigue of existing reinforced concrete bridge deck slabs. Eng Struct 1998;20(11):991–8.
[12] Fathalla E, Tanaka Y, Maekawa K. Remaining fatigue life assessment of in-service road bridge decks based upon artificial neural networks. Eng Struct 2018;171:602–16.
[13] Gebreyouhannes E, Chijiwa N, Fujiyama C, Maekawa K. Shear fatigue simulation of RC beams subjected to fixed pulsating and moving loads. J Adv Concr Technol 2008;6(1):215–26.
[14] Maekawa K, Gebreyouhannes E, Mishima T, An X. Three-dimensional fatigue simulation of RC slabs under traveling wheel-type loads. J Adv Concr Technol 2006;4(3):445–57.
[15] Schläfli M, Brühwiler E. Fatigue considerations in the evaluation of existing reinforced concrete bridge decks. IABSE Proc. IABSE Zurich. 1997. p. 76.
[16] Perdikaris PC, Beim S. RC bridge decks under pulsating and moving load. J Struct Eng 1988;114(3):591–607.
[17] Okada K, Okamura H, Sonoda K. Fatigue failure mechanism of reinforced concrete bridge deck slabs. Transp. Res. Rec. 1978.
[18] FEDRO (The Federal Roads Office), "Annual and monthly results of traffic 2002–2017." 2018 < https://www.astra.admin.ch/astra/en/home/documentation/traffic-data/data-and-publication/swiss-automatic-road-traffic-counts–sartc-/annual-and-monthly-results.html > .
[19] Road construction office (Service des ponts et chaussées), "Weekly traffic distribution, Road construction office. Department of territorial management, Neuchatel Canton."; 2018 (sitn.ne.ch).
[20] Stucki D, Meystre M, Lebet J-P. Updated traffic load for concrete deck slabs of existing bridges. Office fédéral des routes; 2014.
[21] Barr PJ, Stanton JF, Eberhard MO. Effects of temperature variations on precast, prestressed concrete bridge girders. J Bridge Eng 2005;10(2):186–94.
[22] Branco FA, Mendes PA. Thermal actions for concrete bridge design. J Struct Eng 1993;119(8):2313–31.
[23] Elbadry M, Ghali A. Nonlinear temperature distribution and its effects on bridges | heat transfer | convection. Scribd 1983.
[24] Priestley MJN. Thermal gradients in bridges, some design considerations. N Z Eng 1972;27(7):228–33.
[25] Zhu X, Dai Z, Ling J, Chen L. Thermal expansion prediction of cement concrete based on a 3D micromechanical model considering interfacial transition zone. Constr Build Mater 2018;171:891–900.
[26] El-Tayeb EH, El-Metwally SE, Askar HS, Yousef AM. Thermal analysis of reinforced concrete beams and frames. HBRC J 2017;13(1):8–24.
[27] Shen L, Ren Q, Zhang L, Han Y, Cusatis G. Experimental and numerical study of effective thermal conductivity of cracked concrete. Constr Build Mater 2017;153:55–68.
[28] Mottershead JE, Friswell MI. Model updating in structural dynamics: a survey. J Sound Vib 1993;167(2):347–75.
[29] Liu Y, Tan Z, Yang C. Refined finite element modeling of a damaged bridge with virtual distortion method coupling solid superelement. Mech Syst Signal Process 2017;93:559–77.
[30] Schläfli M, Brühwiler E. Test Report 'Fatigue of reinforced concrete elements without shear reinforcement; 1999.
[31] SIA 269, Existing structures – Concrete structures. Zurich: Swiss society of engineers and architects; 2013.
[32] CEB.FIP, fib Model Code for Concrete Structures 2010. Paul Beverly, U. K; 2010.
[33] Johansson U. Fatigue tests and analysis of reinforced concrete bridge. Deck Models 2004.